

A one-dimensional morphoelastic model for burn injuries: sensitivity analysis and a feasibility study

Ginger Egberts · Fred Vermolen · Paul van Zuijlen

November 9, 2021

Abstract

We consider a one-dimensional morphoelastic model describing post-burn scar contractions. This model describes the movement of the skin and the development of the effective Eulerian strain in the tissue. Besides these components, the model also contains components that play a major role in the wound healing process. These components are fibroblasts, myofibroblasts, signaling molecules, and collagen. We perform a sensitivity analysis for many parameters and use the results for a feasibility study. In this study, we test whether the model is suitable for predicting how contraction develops in different age groups. To this end, we conduct an extensive literature review to find parameter values. From the sensitivity analysis we conclude that the most sensitive parameters are the equilibrium collagen concentration in the dermal layer, the apoptosis rate of fibroblasts and myofibroblasts, and the secretion rate of signaling molecules. Further, although we can use the model to simulate distinct contraction densities in different age groups, our results differ from what is seen in the clinic.

1 Introduction

Burns are debilitating, life threatening, and difficult to assess and manage (Lang et al., 2019). Complications after a burn may be a shock, heat exhaustion and heatstroke, infection, and long-lasting distress. Further, all burns, except for superficial burns, lead to scarring. The post-burn scars may be immature/mature, atrophic/hypertrophic/keloid, stable/unstable, depigmented (vitiligo)/hyperpigmented, and may turn malignant as well (Goel and Shrivastava, 2010). Post-burn scars are dry and itchy, and need to be prevented from exposure to sunlight.

One of the common complications in post-burn scars are contractions. Contraction is an active biological process by which an area of skin loss in an open wound is decreased due to concentric reduction in the size of the wound (Goel and Shrivastava, 2010). Wound contraction is a process that continues until the scar is fully matured, and results in a contracture. Depending on the extent of contraction, and the wound dimensions, the contracture can cause limited range-of-motion of joints. This can lead to immobility and is an important indication for scar revision (Egberts et al., 2020). Contractures

may need to be released, which can be done by incision or excision, and immediately or gradually. After this surgery, the area needs to be covered by skin grafts or a skin flap, and postoperative care is mandatory until the graft has become stable.

Burns are so different from other types of wounds that there is a very separate discipline for this class in medical care. There are many different classifications for burns, for example, a burn can be thermal, electrical, or chemical. Burns come with a generalized increase in capillary permeability due to heat effect and damage, and this increase in capillary permeability is not seen in any other type of wound (Tiwari, 2012). Burn wound healing consists of three overlapping phases: inflammation (reactive), proliferation (reparative), and maturation (remodeling). During inflammation, the wound is cleaned and prepared for further protection from bacterial infection. Subprocesses in proliferation are re-epithelialization, angiogenesis, fibroplasia, and wound contraction. The last phase, in which the scar matures and attains a balanced structure, can take years. This results in a scar that, on average, has 50% strength of unwounded skin (within three months), and 80% on the long-term (Enoch and Leaper, 2008; Young and McNaught, 2011).

Within the proliferative phase, fibroplasia encompasses the sub-processes that cause the restoration of the presence of fibroblasts and the production of a new extracellular matrix (ECM) in the injured area (Koppenol, 2017). Fibroblasts can differentiate to myofibroblasts which are responsible for pulling forces in the skin and stimulate, like fibroblasts, both the production of the constituents of the new collagen-rich ECM and the release of metalloproteinases (MMPs). The differentiation of fibroblasts to myofibroblasts is stimulated by transforming growth factor β (Desmoulière et al., 1993). The fibroblasts, the myofibroblasts and collagen deposition play an important role in the wound contraction.

For a long time, mathematical models have been developed that simulate the processes involved in wound healing. These models, (Tranquillo and Murray, 1992; Olsen et al., 1995; McDougall et al., 2006; Koppenol, 2017; Dallon et al., 1999; Barocas and Tranquillo, 1997) to name a few, predict the behavior of experimental and clinical wounds, and gain insight into which elements of the wound healing response might have a substantial influence on the contraction. The majority of the models can be placed into one of three categories: continuum hypothesis-based models, discrete cell-based models and hybrid models (Koppenol, 2017). One of the subcategories of the continuum hypothesis-based models are the mechano-(bio)chemical models. These models together with hybrid models served as a basis for the morphoelastic model that we use in this study and that is developed by Koppenol and Vermolen (2017).

This model is based on the following principle (Hall, 2008): the total deformation is decomposed into a deformation as a result of growth or shrinkage and a deformation as a result of mechanical forces. In a mathematical context, one considers the following three coordinate systems: \mathbf{X} , $\mathbf{X}_e(t)$, and $\mathbf{x}(t)$, which, respectively, represent the initial coordinate system, the equilibrium at time t that results due to growth or shrinkage, and

the current coordinate system that results due to growth or shrinkage and mechanical deformation. Assuming sufficient regularity, the deformation gradient tensor is written by

$$\mathbf{F} = \frac{\partial \mathbf{x}}{\partial \mathbf{X}} = \frac{\partial \mathbf{x}}{\partial \mathbf{X}_e} \frac{\partial \mathbf{X}_e}{\partial \mathbf{X}} = \mathbf{A}\mathbf{Z}, \quad (1)$$

in which the tensor \mathbf{Z} represents the deformation gradient tensor due to growth or shrinkage, and \mathbf{A} represents the deformation gradient due to mechanical forces.

The beauty of this model is that we can simulate a permanent deformation, which results from the contraction process in burn wound healing. The main variable in this model is the displacement of the skin (u), i.e., the variable that makes us able to determine the surface of the wound, and in later stages, the scar. Besides these results, we can also determine the degree of ‘discomfort’ that the patient experiences. We do this by integrating over the entire tissue, including the undamaged part, yielding the total strain energy density. With this we show to what extent there is an elongation in the entire tissue compared to the situation in which there would be no burn. This elongation, which in principle is simply determined by variations in local displacement, may signal nerves, which may cause the patient to experience a nagging sensation. This leads to discomfort in the patient.

The morphoelastic model compromises many parameters. We know some parameter values, while others are unknown and which we need to estimate. Although Koppenol has provided a great overview of parameter values, parameters vary between patients and even along a piece of skin sample. Hence we are interested in both the sensitivity of the parameters and the feasibility of the model. We summarize the change in parameter values that come with aging, and we use the sensitivity analysis results to vary the parameter values along the domain of computation. In our feasibility study, we define distinct classes of patients of different age for which we simulate many burns. The results show the variations in the relative surface area density and the total strain energy density, both for patients of different age.

The organization of this paper is as follows. Section 2 presents the mathematical model and Section 3 presents the numerical method that we use to approximate the solutions. Subsequently, Section 4 presents the parameter values, Section 5 presents the sensitivity analysis, and Section 6 presents the feasibility study. Finally, Section 6 presents the conclusion and discussion.

2 The mathematical model

For the sake of completeness, we present the model that was also used in some of our earlier studies. We model the contraction in burn wounds and scars using partial differential equations that consider the displacement of the dermal layer (u), the displacement velocity of the dermal layer (v), the effective Eulerian strain present in the dermal layer (ϵ) and the changes in distributions of cells and densities of molecules. This morphoelastic continuum hypothesis-based modeling framework comes from Koppenol (2017).

The model follows the assumption from Ramtani and et al (2002) and Ramtani (2004), which state that the Young's modulus of skin depends on the collagen concentration. The model incorporates the evolution in the distributions of fibroblasts (N) and myofibroblasts (M), the concentrations of *signaling molecules* (c) such as cytokines, chemokines, and growth factors, and the collagen concentration (ρ). The one-dimensional differential equations of this framework are

$$\frac{\partial z_i}{\partial t} + \frac{\partial(z_i v)}{\partial x} + \frac{\partial J_i}{\partial x} = R_i, \quad (2)$$

$$\rho_t \left(\frac{\partial v}{\partial t} + 2v \frac{\partial v}{\partial x} \right) - \frac{\partial \sigma}{\partial x} = f, \quad (3)$$

$$\frac{\partial \varepsilon}{\partial t} + v \frac{\partial \varepsilon}{\partial x} + (\varepsilon - 1) \frac{\partial v}{\partial x} = -G. \quad (4)$$

Equation (2) represents the conservation of the distribution/concentration of the constituents $i \in \{N, M, c, \rho\}$ of the dermal layer. Equation (3) is the conservation equation of linear momentum of the dermal layer. Equation (4) is the evolution equation that describes how the effective Eulerian strain, ε , changes. The domain deforms because of the changes in the cells and molecules, and hence the points within the domain of computation are subject to displacement. The second term in the left-hand sides in equations (2) to (4) incorporates this local displacement velocity. The variable z_i in equation (2) represents the distribution/concentration of constituent i , J_i represents the flux of constituent i , and R_i represents the chemical reaction caused by the changes in cell distributions and molecule densities for constituent i . For readability we replace z_i by i , so z_N becomes N , and so on, in the remainder of the text. The constant ρ_t in equation (3) represents the total mass density of the dermal tissues, σ represents the Cauchy stress tensor associated with the dermal layer, and f represents the total body force that works on the dermal layer. The tensor G in equation (4) represents the rate of active change of the effective Eulerian strain.

In the subsequent subsections, we show the fluxes (J), the chemical reactions (R), the mechanical components σ and f and plastic deformation G (i.e., permanent contraction), and the domain of computation, initial conditions and boundary conditions.

2.1 The fluxes of the cells and molecules

For the fluxes of the (myo)fibroblasts we assume that the cells diffuse randomly through the dermal layer according to linear Fickian diffusion. We use the fact that the signaling molecules induce the migration of cells. The fluxes are given by:

$$J_N = -D_F(N + M) \frac{\partial N}{\partial x} + \chi_F N \frac{\partial c}{\partial x}, \quad (5)$$

$$J_M = -D_F(N + M) \frac{\partial M}{\partial x} + \chi_F M \frac{\partial c}{\partial x}. \quad (6)$$

Here the parameter D_F is the (myo)fibroblast diffusion coefficient, which account for random walk, and the parameter χ_F is the chemotaxis coefficient that depends on both

the (un)binding rate of the signaling molecules with its receptor, and the concentration of this receptor on the cell surface of the (myo)fibroblasts. For simplicity we write $N + M = F$ from now on.

The signaling molecules play an important role in the immune and inflammation response after wound healing. While these molecules migrate to the wounded area, they induce directed chemotactic migration of cells. Assuming that the diffusion through the dermal layer follows normal Fickian diffusion, the flux is given by:

$$J_c = -D_c \frac{\partial c}{\partial x}. \quad (7)$$

Here the parameter D_c is the Fickian diffusion coefficient of the signaling molecule.

For collagen, we assume that there is no active transport present, because collagen is attracted to the extracellular matrix instantaneously. Hence:

$$J_\rho = 0. \quad (8)$$

Next, we present the chemical kinetics for the cells and molecules.

2.2 The chemical reactions of the cells and molecules

We incorporate the proliferation of the (myo)fibroblasts into the model using logistic growth models. Signaling molecules also influence the proliferation, differentiation and division of the cells. By taking the signaling molecules into account, the reaction equations are given by:

$$R_N = r_F \left[1 + \frac{r_F^{\max} c}{a_c^I + c} \right] [1 - \kappa_F F] N^{1+q} - k_F c N - \delta_N N, \quad (9)$$

$$R_M = r_F \left[\frac{[1 + r_F^{\max}] c}{a_c^I + c} \right] [1 - \kappa_F F] M^{1+q} + k_F c N - \delta_M M. \quad (10)$$

Here the parameter r_F is the cell division rate, r_F^{\max} is the maximum factor of cell division rate enhancement because of the presence of the signaling molecules, a_c^I is the signaling molecule concentration that causes half-maximum enhancement of the cell division rate, $\kappa_F F$ represents the reduction in the cell division rate because of crowding, q is a fixed constant, k_F is the signaling molecule-dependent cell differentiation rate of fibroblasts into myofibroblasts, δ_N is the apoptosis rate of fibroblasts and δ_M is the apoptosis rate of myofibroblasts.

The stimulation of the differentiation of fibroblasts to myofibroblasts by TGF- β is only effective in the presence of fibronectin and sufficient mechanical stiffness. The proliferation is represented by the first parts on the right-hand side of equations (9) and (10). Myofibroblasts only proliferate in the presence of the signaling molecules, hence the difference between equation (9) and equation (10) in this first part. The differentiation from fibroblasts to myofibroblasts and the apoptosis of the cells are represented by the second

and third parts, respectively. Although myofibroblasts are able to differentiate back to fibroblasts under the influence of Prostaglandin E₂ (PGE₂) (Garrison et al., 2013), we do not take into account the re-differentiation of myofibroblasts to fibroblasts.

Fibroblasts are able to secrete and respond to the signaling molecules. As an addition to this fact we assume that a portion of myofibroblasts also secrete and consume signaling molecules. It is known that MMPs remove signaling molecules from the dermal layer. The MMP concentration depends on the distribution of (myo)fibroblasts, the collagen concentration, and the signaling molecule concentration. MMPs are inhibited by specific tissue inhibitors of metalloproteinases (TIMPs). In line with Koppenol (2017) we assume that the signaling molecules also play an important role in the inhibition. Therefore the chemical reaction equation and MMP concentration (g) are given by:

$$R_c = k_c \left[\frac{c}{a_c^{II} + c} \right] [N + \eta^I M] - \delta_c g(N, M, c, \rho) c, \quad (11)$$

$$g(N, M, c, \rho) = \frac{[N + \eta^{II} M] \rho}{1 + a_c^{III} c}. \quad (12)$$

In equation (11), the parameter k_c is the maximum net secretion rate of the signaling molecules, η^I is the ratio of myofibroblasts to fibroblasts in the maximum secretion rate of the signaling molecules, a_c^{II} is the signaling molecule concentration that causes the half-maximum net secretion rate of the signaling molecules, and δ_c is the proteolytic breakdown rate parameter of the signaling molecules. In equation (12) η^{II} is the ratio of myofibroblasts to fibroblasts in the secretion rate of the MMPs and $1/[1 + a_c^{III} c]$ represents the inhibition of the secretion of the generic MMP. Note that the MMP balance is assumed to be instantaneous.

The amount of collagen is controlled by among others the number of fibroblast and myofibroblasts present in the dermal layer and the signaling molecule concentration. The proteolysis of collagen is like for the signaling molecules related to the MMP concentration. Together, the reaction equation is given by:

$$R_\rho = k_\rho \left[1 + \left[\frac{k_\rho^{\max} c}{a_c^{IV} + c} \right] \right] [N + \eta^I M] - \delta_\rho g(N, M, c, \rho) \rho. \quad (13)$$

Here the parameter k_ρ is the collagen secretion rate, k_ρ^{\max} is the maximum factor of secretion rate enhancement because of the presence of the signaling molecule, a_c^{IV} is the signaling molecule concentration that causes the half-maximum enhancement of the secretion rate and δ_ρ is the degradation rate of collagen.

Next, we present the mechanical component and deformation tensor.

2.3 The mechanical component and deformation tensor

The Cauchy stress tensor is related to the effective Eulerian strain and displacement velocity gradients by a visco-elastic constitutive relation. The body force is generated

by an isotropic stress and a pulling force on the ECM by myofibroblasts. This pulling stress is proportional to the product of the cell density of the myofibroblasts and a function of the collagen concentration. Furthermore, we assume that the rate of active change of the effective Eulerian strain is proportional to the product of the amount of effective Eulerian strain, the local MMP concentration, and the local signaling molecule concentration. Taken together, the Cauchy stress, the body force, and the growth tensor, σ , f , and G , respectively, are given by:

$$\sigma = \mu \frac{\partial v}{\partial x} + E\sqrt{\rho}\varepsilon, \quad f = \frac{\partial \psi}{\partial x}, \quad G = \alpha\varepsilon, \quad \alpha \in \mathbb{R}. \quad (14)$$

Here μ , $E\sqrt{\rho}$, ψ , respectively, represent the viscosity, the Young's modulus (stiffness) and the total stress generated by the myofibroblasts:

$$\psi = \left[\frac{\xi M \rho}{R^2 + \rho^2} \right]. \quad (15)$$

Here the parameter ξ represents the generated stress per unit cell density and the inverse of the unit collagen concentration, and R is a constant. The equation is referred to as activator inhibition (Murray, 2011).

Furthermore, in line with Koppenol, we use

$$\alpha\varepsilon = \zeta \left\{ \frac{[N + \eta^{II}M]c}{1 + a_c^{III}c} \right\} \varepsilon. \quad (16)$$

Here ζ denotes the rate of morphoelastic change.

2.4 The domain of computation, initial and boundary conditions

We define the domain of computation by $\Omega_{x,t}$ with $\partial\Omega_{x,t} = [-L, L]$ the boundary points. We define the wounded area by the subspace $\Omega_{x,t}^w = [-L^w, L^w]$, $L^w < L$ with $\partial\Omega_{x,t}^w = \{-L^w, L^w\}$ the boundary points of the wounded area. Furthermore, we define the steepness of the boundary by s which counts for the slope of the components on the boundary of the wound. The dimension x is in centimeters and t in days.

We use the following function for the initial fibroblast density:

$$N(x, 0) = \begin{cases} \bar{N} & \text{if } x \leq -L^w, \\ \frac{\bar{N} + \tilde{N}}{2} + \frac{\bar{N} - \tilde{N}}{2} \sin\left(\frac{\pi}{s}\left(x + \frac{1}{2}s\right)\right) & \text{if } -L^w \leq x \leq -L^w + s, \\ \tilde{N} & \text{if } -L^w + s \leq x \leq L^w - s, \\ \frac{\bar{N} + \tilde{N}}{2} + \frac{\bar{N} - \tilde{N}}{2} \sin\left(\frac{\pi}{s}\left(x + \frac{1}{2}s\right)\right) & \text{if } L^w - s \leq x \leq L^w, \\ \bar{N} & \text{if } x \geq L^w. \end{cases} \quad (17)$$

Here \bar{N} is the fibroblast density in healthy dermal tissue and \tilde{N} is the fibroblast density in the wounded area.

For the initial signaling molecule concentration, we use the following function:

$$c(x, 0) = \begin{cases} \bar{c} & \text{if } x \leq -L^w, \\ \frac{\bar{c} + \tilde{c}}{2} + \frac{\bar{c} - \tilde{c}}{2} \sin\left(\frac{\pi}{s}\left(x + L^w - \frac{s}{2}\right)\right) & \text{if } -L^w \leq x \leq -L^w + s, \\ \tilde{c} & \text{if } -L^w + s \leq x \leq L^w - s, \\ \frac{\bar{c} + \tilde{c}}{2} + \frac{\bar{c} - \tilde{c}}{2} \sin\left(\frac{\pi}{s}\left(x + 1\frac{1}{2}s - L^w\right)\right) & \text{if } L^w - s \leq x \leq L^w, \\ \bar{c} & \text{if } x \geq L^w. \end{cases} \quad (18)$$

Here \bar{c} is the signaling molecule concentration in healthy dermal tissue and \tilde{c} is the signaling molecule density in the wounded area. Examples of possible initial densities are shown in Figure 1. We use these functions in order to avoid steep changes in the densities. We have assumed that some fibroblasts are present in the wounded area and used that signaling molecules are present in the wounded area due to the secretion by for instance macrophages.

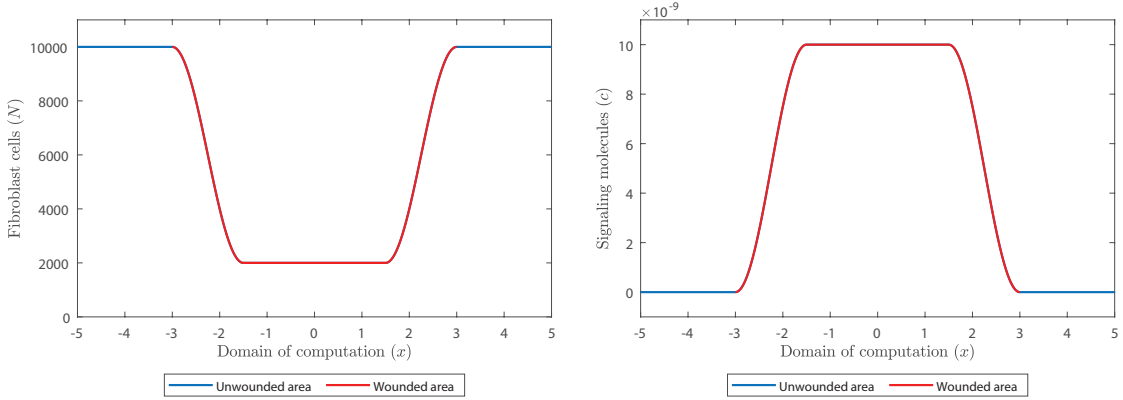


Figure 1: Example of the initial fibroblast density and initial signaling molecule density, with values of the parameters: $L = 5$, $L^w = 3$, $s = 1.5$, $\bar{N} = 10^4$, $\tilde{N} = 2 \times 10^3$, $\bar{c} = 0$ and $\tilde{c} = 10^{-8}$.

In line with Koppenol, we assume that initially no myofibroblasts are present, that a fixed collagen concentration is present, and that the displacement of the dermal layer, the displacement velocity and effective Eulerian strain initially are zero. Hence for all $x \in \Omega_{x,0}$:

$$\begin{aligned} M(x, 0) = \bar{M} = 0, \quad \text{and} \quad \rho(x, 0) = \bar{\rho}, \\ u(x, 0) = 0, \quad v(x, 0) = 0, \quad \text{and} \quad \varepsilon(x, 0) = 0. \end{aligned} \quad (19)$$

We impose the following boundary conditions. For all $x \in \partial\Omega_{x,t}$ and $t \geq 0$:

$$c(x, t) = 0, \quad N(x, t) = \bar{N}, \quad M(x, t) = 0, \quad v(x, t) = 0. \quad (20)$$

The boundary condition for the displacement velocity follows from the assumption that the boundary of computation is sufficient far away from the boundary of the wounded

area. We impose no boundary conditions on the collagen concentration, the displacement of the dermal layer and the effective Eulerian strain.

Next, we show the numerical method that we use to solve the model equations.

3 The numerical method

We approximate the solution to the model equations by the finite-element method using linear basis functions. For more information about this method we refer to Van Kan et al. (2014). Multiplying the partial differential equations (2), (3) and (4) by a test function φ , integration over the domain and the application of Gauß' theorem results in the following equations, where $z = z_i$; $J = J_i$ and $R = R_i$ for readability.

$$\begin{aligned} \int_{-L}^L \left(\frac{\partial z}{\partial t} + \frac{\partial(zv)}{\partial x} - R \right) \varphi - \frac{d\varphi}{dx} J \, dx + [J\varphi]_{-L}^L &= 0, \\ \int_{-L}^L \left(\rho_t \left(\frac{\partial v}{\partial t} + 2v \frac{\partial v}{\partial x} \right) - f \right) \varphi + \frac{d\varphi}{dx} \sigma \, dx - [\sigma\varphi]_{-L}^L &= 0, \\ \int_{-L}^L \left(\frac{\partial \varepsilon}{\partial t} + v \frac{\partial \varepsilon}{\partial x} + (\varepsilon - 1) \frac{\partial v}{\partial x} + \alpha \varepsilon \right) \varphi \, dx &= 0. \end{aligned} \quad (21)$$

Application of the product rule for differentiation and Leibniz-Reynold's transport theorem results in the following variational forms.

Find $z(x, t) \in C^1((0, T]; H^1(\Omega))$, $v(x, t) \in C^1((0, T]; H^1(\Omega))$ and $\varepsilon(x, t) \in C^1((0, T]; L^2(\Omega))$ subject to the given boundary conditions (20) such that

$$\frac{d}{dt} \int_{-L}^L z \varphi \, dx = \int_{-L}^L J \frac{d\varphi}{dx} + R\varphi + z \frac{D\varphi}{Dt} \, dx - [J\varphi]_{-L}^L, \quad (22)$$

$$\rho_t \frac{d}{dt} \int_{-L}^L v \varphi \, dx = \int_{-L}^L \frac{\partial \psi}{\partial x} \varphi - \sigma \frac{d\varphi}{dx} + \rho_t v \frac{D\varphi}{Dt} \, dx + [\sigma\varphi]_{-L}^L, \quad (23)$$

$$\frac{d}{dt} \int_{-L}^L \varepsilon \varphi \, dx + \int_{-L}^L \alpha \varepsilon \varphi \, dx = \int_{-L}^L \varphi \frac{\partial v}{\partial x} + \varepsilon \frac{D\varphi}{Dt} \, dx, \quad (24)$$

for all $\varphi(x, t) \in H_0^1(\Omega)$ and $t \geq 0$. Here $\frac{D\varphi}{Dt} = \frac{\partial \varphi}{\partial t} + v \frac{d\varphi}{dx}$ is the material derivative of the test function φ .

In order to construct the basis functions we subdivide the interval $[-L, L]$ into $n \in \mathbb{N}$ sub-intervals $e_p = [x_p, x_{p+1}]$ (i.e., the elements). Let $X_h(t) = \bigcup_p e_p$ the finite element subspace and $x_j, j \in \{1, \dots, n+1\}$ the vertices of the elements. We choose

$$\varphi_i(x_j, t) = \delta_{ij}, \quad i, j \in \{1, \dots, n+1\} \quad (25)$$

as the linear basis functions. Note that the following transport property holds for the chosen subspace $X_h(t) \subset \Omega_{x,t}$:

$$\frac{D\varphi_i}{Dt} = 0, \quad (26)$$

for all φ_i (Dziuk and Elliot, 2007). The Galerkin equations are simplified using this property.

We perform time integration by the use of backward Euler and we use a monolithic approach with inner Picard iterations. We estimate the displacement of the dermal layer (u) with

$$u_i^{\tau+1} = u_i^\tau + \int_{\tau\Delta t}^{(\tau+1)\Delta t} v(s)ds \simeq u_i^\tau + \Delta t v_i^{\tau+1}. \quad (27)$$

In the next section, we discuss the parameter values.

4 Parameter values

In our search for parameter values, we used various sources from the literature. One of the most important sources is Koppenol's thesis, in which several parameter values have been estimated that we did not find in existing literature. In our study we conduct a sensitivity analysis and a feasibility study. In the Appendix one finds the parameter values that we used in this study. In this chapter, we describe how we chose these values.

Equilibrium values

The estimation of the equilibrium distribution of fibroblasts differs per study. One estimates the number to be about $\mathcal{O}(10^4)$ cells/cm³ (Olsen et al., 1995), and the other estimates the number to be about $\mathcal{O}(10^6)$ cells/cm³ (Miller et al., 2003). The estimation of the number of cells also differs for the papillary and the reticular dermis, where there exist much more fibroblasts in the papillary dermis (Harper and Grove, 1979; Randolph and Simon, 1998). In our simulations we have seen that the model works best with the equilibrium distribution of $\mathcal{O}(10^4)$ cells/cm³. We note that some other parameter values (δ_c, δ_ρ) depend on the chosen order for \bar{N} , since we need to take into account the density of MMPs. Furthermore, research has found that among ages 1-10 the number of fibroblasts is nearly twice as high as in any other postnatal age group (Gunin et al., 2011). Therefore we choose the mean value $\bar{N} = 10^4$ cells/cm³ and let the value decrease with age.

The number of myofibroblasts present in the skin depends on the condition of the skin. Myofibroblasts result from the differentiation of fibroblasts. We assume that myofibroblasts are not present at the beginning of proliferation. This is in line with what Olsen et al. (1995) assume. Hence $\bar{M} = 0$ cells/cm³.

In Olsen et al. (1995), the equilibrium collagen concentration is estimated as follows. Roughly 75% of the 15% of other substances than water and fat in 1 ml of human dermal tissue is collagen. This yields $\bar{\rho} \approx 0.75 \times 0.15 \text{ g ml}^{-1} = 0.1125 \text{ g ml}^{-1}$. Furthermore, in human skin collagen content decreases at about 2% per year (Farage et al., 2015).

Therefore we choose the mean value $\bar{\rho} = 0.1125 \text{ g/cm}^3$ and let the value decrease with age.

Taking into account the reaction term for the signaling molecules (11), and the equilibria \bar{N} , \bar{M} and $\bar{\rho}$, the equilibrium density of the signaling molecules should be $\bar{c} = 0 \text{ g/cm}^3$.

Initial values

When the skin burns, the cells also burn away. Immediately after the burn, the body attracts signaling molecules to the wound area, after which it attracts fibroblasts to the wound. Since we simulate from the onset of proliferation, we assume that several fibroblasts are present. We let this number be 20 percent of the equilibrium number. So the mean value is $\tilde{N} = 2 \times 10^3 \text{ cells/cm}^3$.

Due to the supply of growth factors in the inflammatory phase, the initial signaling molecule concentration is unequal to zero. The value should not exceed $15\text{-}50 \text{ ng ml}^{-1}$ (Olsen et al., 1995), and is therefore chosen to be $\tilde{c} = 10^{-8} \text{ g/cm}^3$.

Flux values

In Sillman et al. (2003), the migratory rates of fibroblasts varied depending on the experimental medium used: in serum-containing medium the average velocity was as low as 0.23 mm/min , while in serum-free keratinocyte medium the average velocity was as high as 0.36 mm/min . Hence, in serum-containing medium the rate was $7.6176 \times 10^{-7} \text{ cm}^2/\text{day}$ and in serum-free keratinocyte medium the rate was $1.86624 \times 10^{-6} \text{ cm}^2/\text{day}$. All the reported values together yield a mean value of $1.3247 \times 10^{-6} \text{ cm}^2/\text{day}$ and standard deviation $3.7823 \times 10^{-8} \text{ cm}^2/\text{day}$. However, in Olsen et al. (1995); Simpson et al. (2017), the estimates are $1.44 \times 10^{-5} \text{ cm}^2/\text{day}$ and $1.2 \times 10^{-5} \text{ cm}^2/\text{day}$ respectively. We therefore estimate the value of D_F to be around $10^6 \text{ cm}^5/(\text{cells day})$. Furthermore, we assume that the diffusion of (myo)fibroblasts decreases with age.

For the chemotactic parameter χ_F we adopt the value from Murphy et al. (2012), which is $2 \times 10^{-3} \text{ cm}^5/(\text{cells day})$ and for the diffusion parameter D_c we adopt the value from Haugh (2006), which is approximately $2.88 \times 10^{-3} \text{ cm}^2/\text{day}$. Furthermore, we assume that the diffusion of signaling molecules decreases with age.

Chemical kinetics values

Cell doubling time can be calculated using the growth rate (amount of doubling in one unit of time) in the following way: doubling time = $\ln(2)/\text{growth rate}$. The average doubling time for fibroblasts is approximately 18-20 h (Alberts et al., 1989; Gosh et al., 2007). This gives the range for the proliferation rate of $0.832 \leq r_F \leq 0.924$. We choose the upper limit, hence $r_F = 0.924 \text{ cm}^{3q}/(\text{cells}^q \text{ day})$. Furthermore, Gunin et al. (2011) show that the percentage of PCNA-positive fibroblasts decreases with age, and that PCNA can be considered as a marker for the proliferating cells. We therefore let the cell division decrease with age.

TGF- β increases fibroblast proliferation by 2-3 times (Strutz, 2001). We choose the upper limit, hence $r_F^{\max} = 2$.

The chemical concentrations required to enhance fibroblast proliferation are somewhat higher than those for chemotactic responses (Grotendorst, 1992). Experimental evidence indicates that half-maximal enhancement corresponds to concentrations about 10 ng per ml (Olsen et al., 1995). We adopt this value and take $a_c^I = 10^{-8}$ g/cm³.

The carrying capacity of fibroblasts is known to be approximately $\kappa_F = 10^{-6}$ cm³/cells (Vande Berg et al., 1989), a value that we adopt. Furthermore, skin becomes thinner with age and therefore we assume that crowding occurs faster in elderly. Hence we let the division rate reduction value increase with age.

We need to have a stable chemical reaction (i.e., $R_i = 0$) in case the cell distributions and molecules densities are in equilibrium. The constant q gives us the opportunity to have a stable reaction in equilibrium for equation (9). Given the equilibria, solving $R_N = 0$ for q yields:

$$q = \frac{\log(\delta_N) - \log(r_F(1 - \kappa_F \bar{N}))}{\log(\bar{N})}. \quad (28)$$

In Desmoulière et al. (1993), culturing fibroblasts in the presence of TGF- β increased the percentage of cells expressing α -SMA from 7.5% to 45.3%, representing an activation of 37.8% of myofibroblast type cells. This experiment occurred over one week period, with a TGF- β dose of 5-10 ng per ml. Suppose the activation of myofibroblasts follows a linear equation. Then given $y(7) = 7a = 0.378$, we have $a = 0.054/\text{day}$. A dose of 5-10 ng per ml yields $0.054/10 \times 10^{-9}$ and $0.054/5 \times 10^{-9}$ cm³/(g day), giving the range $5.4 \times 10^6 \leq k_F \leq 1.08 \times 10^7$ cm³/(g day). We choose the upper limit. Furthermore, Simpson et al. (2009) demonstrated a failure of fibroblast-myofibroblast differentiation and showed that this is associated with in vitro aging. Hence we let the differentiating parameter decrease with age.

The average fibroblast doubling time (DT) ranges from 18-20 h (Alberts et al., 1989; Gosh et al., 2007), and the average lifespan of fibroblasts varies between 40 and 70 population doublings (PD) (Azzarone et al., 1983; Moulin et al., 2011). Using the formula

$$\delta_N = (\ln 2)/(PD \times DT/24), \quad (29)$$

we end up with the range $0.0119 \leq \delta_N \leq 0.0231$. We choose the value $\delta_N = 0.02/\text{day}$ and let this value decrease with age, since on average, the doubling time of fibroblasts decreases with age (Simpson et al., 2009).

In a previous study for hypertrophic scars, Koppenol et al. (2016) estimated the apoptosis rate of myofibroblasts. Within this study it was found that a value of $\delta_M = 0.002$ /day corresponds to hypertrophic scars and that a value of $\delta_M = 0.06$ /day corresponds to normal scars. Furthermore, Moulin et al. (2003) provide means of percentages: 8.85% for normal scars and 1.06% for hypertrophic scars. Combination of these results yield

the range $0.06 \leq \delta_M \leq 0.0885$ for normal scars and $0.0106 \leq \delta_M \leq 0.02$ for hypertrophic scars. For our study we take the lower value $\delta_M = 0.06/\text{day}$ for normal scars.

Olsen et al. (1995) relate the inhibitor of TGF- β to the initial concentration of the growth factors so that $a_c^{II} = 10^{-8} \text{ g/cm}^3$. We adopt this value.

Myofibroblasts produce roughly twice the collagen that is synthesized by fibroblasts (Rudolph and Vande Berg, 1991). Hence the constant $\eta^I = 2$.

The half-life of TGF- β is about 2 minutes (Wakefield et al., 1990), and the half-life of PDGF is about 2 minutes as well (Bowen-Pope et al., 1984). So signaling molecules have a decay rate of $-\log(0.5^{24 \times 60/2}) \approx 499/\text{day}$. However, Olsen et al. (1995) decrease the value for two reasons: not all signaling molecules may bind, for example because of insufficient levels of binding protein present at the wound site, and the bound complex may be recognized by (myo)fibroblasts leading to internalized and metabolized signaling molecules. Therefore, the estimated decay rate is $0.5/\text{day}$. Other estimates for TGF- β are $0.462 - 0.693/\text{day}$ (Javierre et al., 2009) and $0.354/\text{day}$ (Yang et al., 1999; Murphy et al., 2012). Given our equilibrium parameter values, the MMP density has order of magnitude $\mathcal{O}(\bar{N}) \times \mathcal{O}(\bar{\rho}) = \mathcal{O}(10^3)$. Hence taking care of the equilibrium dimensions of the model, we end up with a range of $(3.54 - 6.93) \times 10^{-4} \text{ cm}^6/(\text{cells g day})$. We take the value $\delta_c = 5 \times 10^{-4} \text{ cm}^6/(\text{cells g day})$.

From our previous stability analysis (Egberts et al., 2020) it follows that $k_c \leq \delta_c \bar{\rho} a_c^{II}$. Given the parameter values, we set $k_c = 3 \times 10^{-13} \text{ g}/(\text{cells day})$.

We estimate the constant $\eta^{II} = 0.45$, which is a small deviation from the constant estimated in Koppenol (2017).

From Overall et al. (1991), this value is estimated to be between $(2 - 2.5) \times 10^8 \text{ cm}^3/\text{g}$. We choose the lower limit, hence $a_c^{III} = 2 \times 10^8 \text{ cm}^3/\text{g}$. Furthermore, the production of matrix metalloproteinases (MMPs) increases with age (Ashcroft et al., 1997). Since the numerator in equation (12) is decreasing with age we assume that the increase in production is because of a decrease in inhibition. Hence, we let the inhibition factor decrease with age.

The secretion rate of collagen k_ρ gives us the opportunity to have a stable reaction in equilibrium for equation (13). Given the equilibria, solving $R_\rho = 0$ for k_ρ yields:

$$k_\rho = \delta_\rho \bar{\rho}^2. \quad (30)$$

The synergistic effects of growth factors may accelerate collagen biosynthesis up to ten-fold (Olsen et al., 1995). Hence $k_\rho^{\max} = 10$.

Data from Roberts et al. (1986) suggest that half-maximal enhancement of collagen synthesis occurs at TGF- β concentrations of the order of 1 ng per ml . We adopt this value, so $a_c^{IV} = 10^{-9} \text{ g/cm}^3$.

For the decay rate of collagen we adopt the estimated value from Koppenol et al. (2016). Furthermore, according to Farage et al. (2015), the collagen turnover decreases with age. Hence we set $\delta_\rho = 6 \times 10^{-6} \text{ cm}^6/(\text{cells g day})$ and let the proteolytic breakdown of collagen decrease with age.

Mechanical values

Koppenol and Vermolen (2017) estimated the viscosity value to be of order $O(10^2)$ for the two-dimensional morphoelastic model. In our previous study (Egberts et al., 2020), the stability analysis showed that $\mu \geq \frac{\sqrt{\rho E}}{\pi}$ must hold for the one-dimensional morphoelastic model. Given other parameter values we can adopt the value $\mu = 100 \text{ (N day)/cm}^2$. Furthermore, since the viscosity is constant up to 40s and increases a little after turning 40 (Xu and Tianjian, 2011), we let the viscosity increase with age.

We estimate that the constant E in the Young's Modulus $E\sqrt{\rho}$ is $350 \text{ N}/((\text{g cm})^{\frac{1}{2}})$ for the one-dimensional morphoelastic model and let this value increase with age (Pond et al., 2018; Pawlaczyk et al., 2013).

For the parameters in the body force, we adopt the values from Koppenol and Vermolen (2017). That is $\xi = 4.4 \times 10^{-2} \text{ (N g)/(cells cm}^2\text{)}$ (Maskarinec et al., 2009) & (Wrobel et al., 2002), $R = 0.995 \text{ g/cm}^3$, and $\zeta = (0 - 9) \times 10^2 \text{ cm}^6/(\text{cells g day})$. We set $\zeta = 4 \times 10^2/(\text{cells g day})$ and let this value increase with age, because the skin's ability to recover after stretching decreases over lifetime (Krueger and Luebberding, 2017).

Last, but not least, Table A.1 in Wrobel et al. (2009) shows that $\rho_t = 1.09 \text{ g/cm}^3$ for human skin. We adopt this value.

Next, we present our sensitivity analysis.

5 Sensitivity analysis

The model compromises 34 parameters of which we vary the following 30 to study the sensitivity of these parameters:

- the equilibria \bar{N} and $\bar{\rho}$, and the initial conditions \tilde{N} , \tilde{c} and $\tilde{\rho}$;
- the apoptosis rates δ_N and δ_M , and the decay rates δ_c and δ_ρ ;
- the parameters responsible for enhancement of cell division and molecule secretion a_c^I , a_c^{II} and a_c^{IV} , and the inhibition of MMP secretion a_c^{III} ;
- the ratios from myofibroblasts to fibroblasts η^I and η^{II} , and chemokine dependent differentiation rate k_F ;
- the diffusion and chemotaxis rates D_F , D_c and χ_F ;
- the proliferation and secretion rates r_F and k_c , and the maximum factors r_F^{\max} and k_ρ^{\max} ;

- the crowding factor κ_F ;
- the parameters ξ and R that influence the force;
- the viscosity μ , Young's-Modulus factor E , morphoelastic factor ζ , and the total mass density of dermal tissues ρ_t .

We also variate the length of the initial wound L^w . The analysis is organized as follows. For each chosen parameter we vary the value by decreasing or increasing it by $\pm 0, 5, 10, 15, 20, 25\%$. This means we perform 341 simulations. Namely, for each parameter we perform 11 simulations while leaving the values of the other parameters at the mean value. The mean values are given in Tables 3a - 3d, where in Tables 3c and 3d the mean values are given in the third column (μ^2).

We are interested in the contraction during wound healing and scar formation, and in the total strain energy density. The latter is assumed to be a measure for the discomfort that the patient experiences and is defined by

$$E_\varepsilon(t) = \int_{-L}^L \frac{1}{2} E \sqrt{\rho(x,t)} \varepsilon(x,t)^2 dx = \int_0^L E \sqrt{\rho(x,t)} \varepsilon(x,t)^2 dx. \quad (31)$$

Here we used the symmetry of the domain.

The results show the *minimum of the relative surface area* (RSA_{min}) (i.e., maximum contraction value) in a time period of one year, the *day on which the minimum relative surface area is reached* (RSA_{day}) (i.e., the day after which the wound/scar retracts), the *relative surface area on day 365* (RSA_{365}), the *maximum value of the strain energy density* (SED_{max}), and the *day on which the maximum value of the strain energy density is reached* (SED_{day}) (i.e., the day after which the patient experiences a reduction in discomfort due to the internal stress in the skin). In our simulations we used $L = 10$ cm for the boundary of the domain of computation and the mean value $L^w = 3.6$ cm for the wounded area.

Given the values in $r \in \{RSA_{min}, RSA_{day}, RSA_{365}, SED_{max}, SED_{day}\}$ for a variation $j \in \{-25\%, \dots, +25\%\}$, we compute the *z-scores* for the parameter $i \in \{\bar{N}, \dots, L^w\}$. The basic *z-score* for a sample is $z = (x - \bar{x})/s_x$, where \bar{x} is the sample mean and s_x is the sample standard deviation.

We define the measure for sensitivity by summing over the absolute values of the *z-scores* as follows:

$$\mathcal{S}_i^r = \sum_j |z_{ij}^r|, \quad (32)$$

where z_{ij}^r is the *z-score* of the data in r for parameter i in variation j . For example, $z_{\delta_N, 15\%}^{RSA_{365}}$ represents the *z-score* of the relative surface area on day 365 for parameter δ_N in the simulation where the value for δ_N is increased with 15%.

Table 1 gives an overview of the sensitivity values in terms of *z-scores* for the 31 parameters that we varied. In the last column we rounded the sum of the values. From this table

Parameter	$\mathcal{S}^{RSA_{min}}$	$\mathcal{S}^{RSA_{day}}$	$\mathcal{S}^{RSA_{365}}$	$\mathcal{S}^{SED_{max}}$	$\mathcal{S}^{SED_{day}}$	\mathcal{S}^{total}
\bar{N}	9.207	8.835	9.496	10.349	7.58	45
$\bar{\rho}$	20.351	33.916	15.383	29.19	30.21	129
\tilde{N}	3.347	2.959	1.979	3.813	3.321	15
\tilde{c}	3.687	3.015	2.065	2.721	4.544	16
$\tilde{\rho}$	1.418	3.107	1.765	2.991	2.048	11
δ_N	22.549	11.747	23.891	17.851	15.05	91
δ_M	20.52	11.794	23.787	17.245	11.423	85
δ_c	12.001	9.09	11.558	5.1	16.287	54
δ_ρ	8.905	15.125	6.879	13.054	13.552	58
a_c^I	4.496	9.211	5.731	10.169	2.257	32
a_c^{II}	4.828	2.057	4.779	2.823	4.499	19
a_c^{III}	8.929	10.753	8.912	11.091	8.917	49
a_c^{IV}	2.306	3.107	1.529	2.991	3.037	13
η^I	8.175	3.364	8.227	4.821	8.248	33
η^{II}	6.551	5.713	9.24	6.304	5.607	33
k_F	1.329	7.903	2.324	8.49	2.259	22
D_F	1.954	2.057	1.604	1.867	2.427	10
D_c	2.154	3.015	1.595	2.882	2.297	12
χ_F	1.817	3.107	1.598	2.991	2.512	12
r_F	4.649	1.486	3.69	2.301	4.07	16
k_c	16.993	15.121	14.234	10.024	22.49	79
r_F^{\max}	17.546	9.879	18.152	13.054	12.097	71
k_ρ^{\max}	8.268	12.692	6.455	11.591	12.036	51
κ_F	1.89	3.107	1.573	2.991	2.551	12
ξ	14.892	2.057	14.571	1.18	11.62	44
R	20.174	10.753	21.508	13.568	13.648	80
μ	1.782	3.107	1.6	2.991	2.423	12
E	13.306	4.157	6.397	4.94	8.485	37
ζ	3.845	5.098	1.728	2.991	10.851	25
ρ_t	1.817	3.107	1.598	2.991	2.512	12
L^w	2.038	9.173	11.521	9.795	4.011	37

Table 1: Sensitivity of the varied parameters in terms of z -scores

we can see that the parameter that represents the equilibrium collagen concentration ($\bar{\rho}$) with score 129 is the most sensitive. It is therefore interesting to study the equilibrium collagen concentrations in human skin, since collagen concentrations decrease with age (Farage et al., 2015) and we use this value for our age study in the next section. Parameters that are the least sensitive are the diffusion rate of (myo)fibroblasts (D_F) with score 10 and the initial collagen concentration ($\tilde{\rho}$) with score 11. Concerning the diffusion D_F , we must note that the mean value is of order $\mathcal{O}(10^{-6})$, which is different from the order used in Koppenol (2017), where it is of order $\mathcal{O}(10^{-7})$. This may lead to stating that this parameter is not sensitive to variations, while in a different geometry it might be much more sensitive. Concerning the initial collagen concentration ($\tilde{\rho}$), we note that the value is varied when the equilibrium collagen concentration is fixed to the mean value ($\bar{\rho} = 0.1125$). In case the equilibrium collagen concentration $\bar{\rho}$ is varied, the parameter for the initial collagen concentration is fixed to 20% of 0.1125, which is the mean value of $\bar{\rho}$ and not the variation.

Other parameters that seem significantly sensitive are the apoptosis of fibroblasts (δ_N) with score 91, the apoptosis of myofibroblasts (δ_M) with score 85, the constant R that influences the force with score 80, and the secretion of signaling molecules (k_c) with score 79. However, we must note that the mean values for δ_M , R and k_c are estimated in Koppenol (2017) for a two-dimensional setting in which other values for parameters were used. Furthermore, the value of k_c is based on a stability criterium that was found in our previous stability analysis (reference to other paper):

$$k_c \leq \delta_c a_c^{II} \bar{\rho}, \quad (33)$$

and since the parameter for the equilibrium collagen concentration is sensitive, it is not a surprise that this secretion parameter is also sensitive. The value for the secretion of chemokines is not that straightforward. The secretion value of cytokines is different from the secretion value of growth factors and yet we model these together in one variable c representing chemokines. In order to prevent the model from unnecessary complicated computations, we continue modeling with this simplification and bear in mind the sensitivity of the parameter k_c . It is therefore also interesting to study the rates of apoptosis of fibroblasts, since the doubling time of fibroblasts decreases with age (Simpson et al., 2009) and we use this value for our age study in the next section.

Figures 2 and 3 visualize the effect of the variations in the parameters. In order to have a clear distinction between the sensitive parameters and other parameters, there is no legend, and the most important lines are labeled and have different styles. Figure 2 shows, for example, that for smaller values of δ_N (the apoptosis rate of fibroblasts) the relative surface area is larger and that for larger δ_N the relative surface area is smaller. A smaller surface area corresponds with more intense contraction. From the plots it is clear that decreasing the equilibrium collagen concentration leads to an increased healing time. Namely, the day on which the maximum contraction is reached is moved forward with 49 days yielding 11.5% more contraction on day 365. The sensitivity of this parameter is also visible in the plots representing the strain energy density. However,

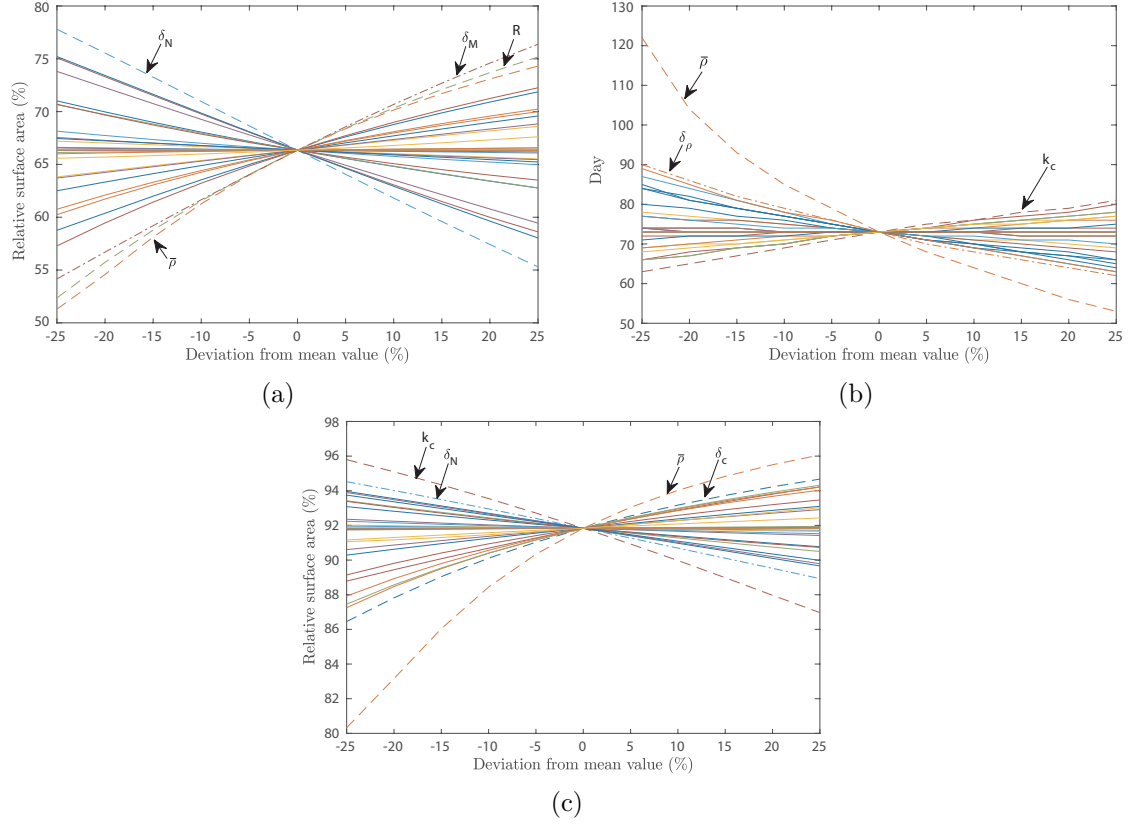


Figure 2: Effects of the variations in parameters for the relative surface area. Shown are the effects on the minimum of the relative surface area (a), the effects on the day on which the minimum of the surface area is reached (b), and the effects on the relative surface area on day 365 (c)

here the apoptosis of myofibroblasts δ_M and constant R (a measure for inhibition) have a larger effect for the variations $-15, -10, -5, +5, +10, +15, +20, +25\%$.

We use the results from the sensitivity analysis to perform a feasibility study in the next chapter.

6 Feasibility study of modeling age dependent scar/skin contraction

To study the feasibility of age-dependent uncertainty quantification, we focus on the effect of aging of skin on contraction, the final contracture, the total strain energy density, and the maximum of the total strain energy density. Just like any other organ, aging also affects the skin. Aging has a delaying effect on wound healing and immune responses. Intrinsic aging is the effect of generic and internal influences, such as hor-

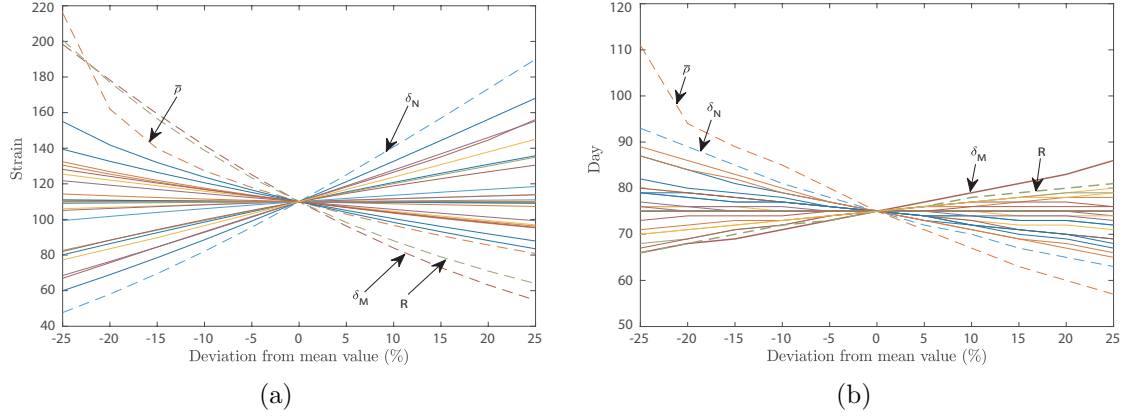


Figure 3: Effects of the variations in parameters for the total strain energy density. Shown are the effects on the maximum of the total strain energy density (a) and the effects on the day on which the maximum of the total strain energy density is reached (b)

mones or metabolic substances. Extrinsic aging is the effect of external influences, such as UV radiation and environmental toxins (Wiegand et al., 2017). Clear general signs of aging are wrinkles, sagging skin and pigmentary irregularities, and increased tendencies to injuries and the faster opening of healing wounds. These symptoms result from physiological changes such as decreased cell replacement rate. We therefore review various sources from literature to find suitable values for the parameters of the model. In this way we can perform simulations for patients of different ages. Based on the results found, we have chosen the classes that are presented in Table 2.

Class	Age
1	0 - 15
2	16 - 40
3	41 - 70
4	71+

Table 2: Classes of patients of different age

In this study, there are five groups of parameters:

1. parameters that are constant along the patients and not varied along the domain of computation,
2. parameters that are constant along the patients and varied along the domain of computation,
3. parameters that are varied along the patients and not varied along the domain of computation,

4. parameters that are varied along the patients and varied along the domain of computation,
5. parameters that are dependent on other parameters.

To assess the uncertainty in the input data, we use a basic Monte Carlo method in which we sample input data from predefined statistical distributions. Regarding spatially heterogeneous parameters, we use sampling from a log-normal distribution. Each sample is a one-dimensional realization, and is based on the heterogeneous sampling through a normalized truncated Karhunen-Loéve expansion of a zero-mean stochastic process, by

$$\hat{u}(X) = \sum_{j=1}^n \hat{Z}_j \sqrt{\frac{2}{n}} \sin \left((2j-1) \frac{\pi}{2|\Omega_{x,t}|} X \right), \quad (34)$$

where $\hat{Z}_j \sim \mathcal{N}(0, 1)$, hence \hat{Z}_j denotes a set of *iid* stochastic variables that follow the standard normal distribution, $|\Omega_{x,t}|$ is the length of the domain of computation, and $-L \leq X \leq L$. From the stochastic variable $\hat{u}(X)$, we show the regeneration of, for example, \hat{E} by

$$\log(\hat{E}(X)) \sim \mu + \sigma \hat{u}, \quad (35)$$

so

$$\hat{E}(X) = \exp(\mathcal{M}_E + \mathcal{S}_E \hat{u}(X)). \quad (36)$$

Hence $\hat{E}(X)$ is a realization of a *lognormal* distribution with mean \mathcal{M}_E (expected value) and standard deviation \mathcal{S}_E . These values can be expressed by the arithmetic (sample) mean μ_E and arithmetic standard deviation σ_E as follows

$$\mathcal{M}_E = \ln \left(\frac{\mu_E}{\sqrt{1 + \frac{\sigma_E^2}{\mu_E^2}}} \right), \quad \text{and} \quad \mathcal{S}_E = \sqrt{\ln \left(1 + \frac{\sigma_E^2}{\mu_E^2} \right)}. \quad (37)$$

In the same way, we can create heterogeneous, stochastic inputs for other parameters as well.

We test the null-hypothesis $H_0 : \mu_A = \mu_B$ versus a two-sided alternative for classes A and B of patients using the following t -statistic:

$$t = \frac{\bar{X}_A - \bar{Y}_B}{s_p}, \quad s_p = \sqrt{\frac{s_a^2 + s_b^2}{n_b}}$$

where \bar{X}_A and \bar{Y}_B are the mean values of the results in distinct age groups A and B , s_p is the estimated standard error of $\bar{X}_A - \bar{Y}_B$, s_a^2 and s_b^2 are the standard deviations in the age groups A and B , and n_b is the number of samples in the age groups. Here we assume that the number of samples in the age groups are equal. We reject the null-hypothesis if $|t| > t_{2(n_b-1)}(\alpha/2)$, with $\alpha = 0.001$.

In the Appendix one finds Table 3 that shows the chosen parameter values as well as the standard deviation values for the variation over the domain of computation (if applicable).

Next, we present the simulation results. To reduce the computation time, we performed simulations on half a domain $\Omega^{1/2} = [-L, 0]$ with $L = 10$ cm. In all simulations $L^w = 3.6$ cm, hence the initial wounded area $\Omega_{x,0}^w = [-3.6, 0]$.

We simulated $n_b = 1950$ burns per age group. Hence, in total we simulated 7800 burns. We used parallel computing with 12 processors, three processors responsible per group, on a 64 bit Windows 10 Pro system with 16 GB RAM and 3.59 GHz AMD Ryzen 5 3600 6-Core Processor. The total computation time was 13.5 hours, hence the mean computation time per simulation takes less than half a minute. A major advantage of the one-dimensional implementation is its short computation time, which allows to do many of them within a reasonable time interval. For the test statistic, we used $t_{3898}(0.0005) = 3.293$. The standard deviations $s_{i,m}^2$ for the age classes $i \in \{1, 2, 3, 4\}$ for the minimum of the relative surface area (i.e., maximum contraction) are

$$s_{1,m}^2 = 1.2158, \quad s_{2,m}^2 = 1.1293, \quad s_{3,m}^2 = 1.2570, \quad \text{and} \quad s_{4,m}^2 = 1.2815.$$

The standard deviations $s_{i,e}^2$ for the age classes $i \in \{1, 2, 3, 4\}$ for the relative surface area on day 365 are

$$s_{1,e}^2 = 0.2941, \quad s_{2,e}^2 = 0.3105, \quad s_{3,e}^2 = 0.4003, \quad \text{and} \quad s_{4,e}^2 = 0.4238.$$

Figure 4 shows four 95% confidence intervals for the mean of the size of the scar. Each confidence interval corresponds to a group of patients. The range of the contraction values comes from the variability of the parameters over the domain of computation. From Figure 4, it can be seen that the maximum contraction value (i.e., minimum of the relative surface area) is about the same in the first two groups of ages and from group 2, a higher age class gives a larger reduction of the size of the scar, and therewith a larger intensity of the contraction. Further, for higher ages, it takes more time to reach the maximum intensity of contraction. There seems to be more variability in the permanent deformation in the elderly patients. Furthermore, it seems that in elderly patients it takes longer before the wound healing cascade reaches equilibrium than in younger patients. Minima of the relative surface area were mostly reached on days 34, 61, 74, and 95, with values of 76.7, 76.0, 74.4, and 72.9% for groups 1, 2, 3, and 4, respectively. Unfortunately, these results do not correspond fully to the observations in the clinic. Normally, contraction is of less order in elderly patients and, in general, retraction takes a longer period. We note that the longer retraction period is visible in the two-dimensional model results in Koppenol and Vermolen (2017) and is handled with the parameter a_c^{III} . Furthermore, in clinic one sees more contractures in younger patients. This is because of a variety of factors that have not been modeled in our mathematical model yet.

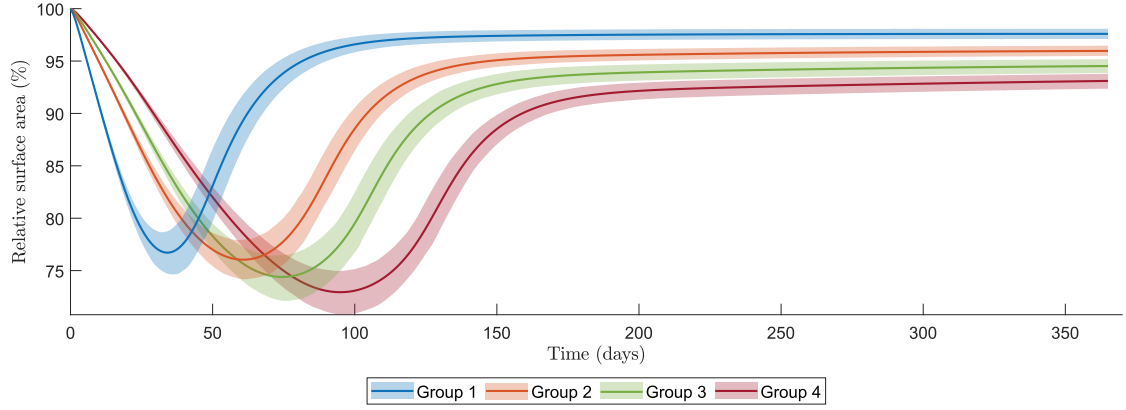


Figure 4: Confidence intervals for the contraction of burns in different age groups. The intervals show the mean values and the 95% confidence values of the mean

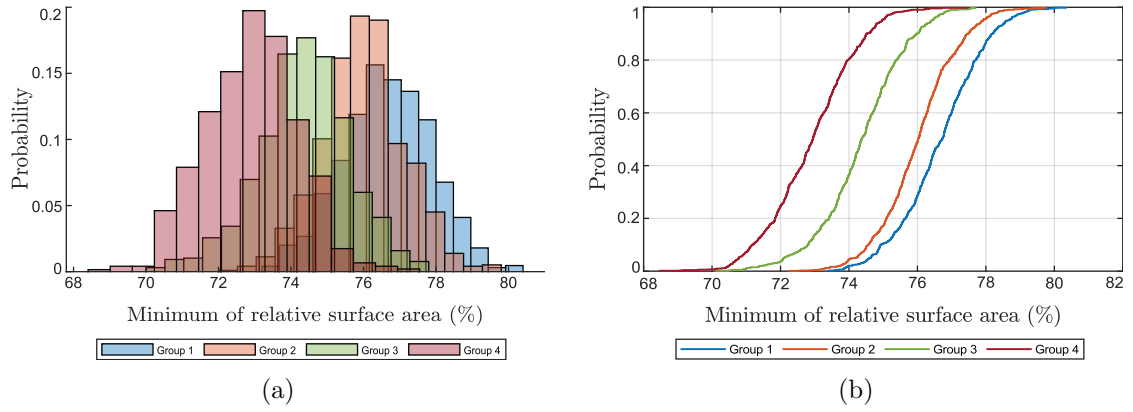


Figure 5: Histograms of the minimum relative wound area (a) and its cumulative distribution function (b)

Figure 5 shows the results on the minimum relative surface area (i.e., maximum of contraction). Although we see that there is an overlap between all the groups, the maximal contraction is significantly different ($p < 0.01$) between the groups (see Table 4a in the Appendix). This overlap is also visible in the estimated cumulative distribution function plot on the right, where the functions of the first and second group, and the third and fourth group, almost intersect. From the cumulative distribution functions we can estimate the probabilities of reaching a certain amount of maximum contraction. For example, this figure suggests that with 70% probability a patient from groups of patients 1, 2, 3, and 4, respectively, can reach 22.7% contraction, 23.5% contraction, 25.1% contraction, and 26.4% contraction.

Figure 6 shows the results on the permanent contraction. The relative surface area is an indicator for the final contracture. We see that there is an overlap between all the groups, where the first and last group have the least overlap. Further, the younger the

patients, the lower the probabilities. However, the overlap between the groups for the final contraction value is less than for the maximum contraction value. This can be seen in the right plot, where the cumulative distribution functions seem to be more separated. The histograms also show a correlation between aging and the spread, confirming the observation found in the confidence intervals, that there is larger variability in the contractures in elderly people than in children. Mean values for the final contraction are 97.4%, 95.8%, 94.5%, and 93.3% for groups 1, 2, 3, and 4, respectively.

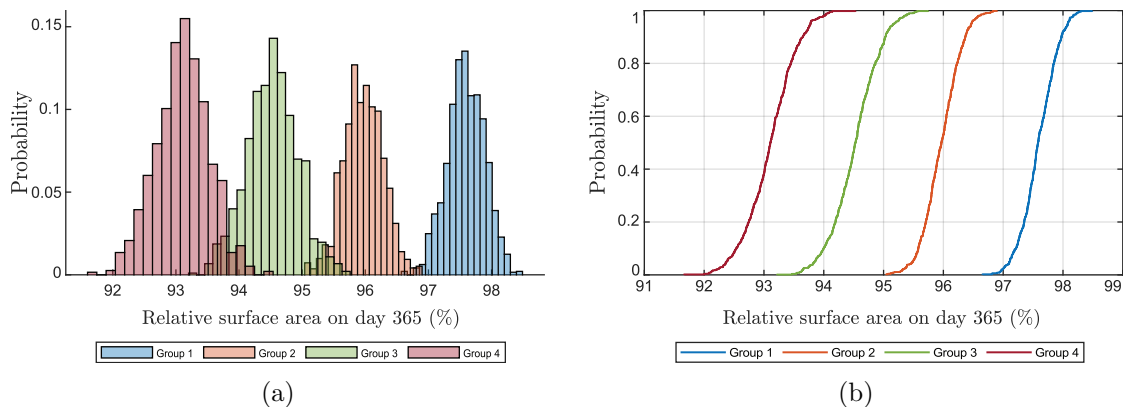


Figure 6: Histograms of the relative surface area on day 365 (a) and its cumulative distribution function (b)

Figure 7 shows four confidence intervals for the mean of the total strain energy density. Each confidence interval corresponds to a group of patients. The range of the total strain energy density comes from the variability of the parameters over the domain of computation. From Figure 7, it can be seen that the maximum of the total strain density is about the same in the first two groups of ages and from group 2, a higher age class gives a larger maximum of the total strain energy density. Further, for higher ages, it takes more time to reach the maximum total strain energy density. Note that all these results are related to the relative surface area densities shown in Figure 4. Maxima of the total strain energy density were mostly reached on days 36, 64, 78, and 95, with values of 62, 66, 74 and 79 for groups 1, 2, 3, and 4, respectively. We note that the maximum of the total strain energy density is reached a few days later than the maximum contraction in almost all groups.

Figure 8 shows the results on the maximum of the total strain energy density. Like in Figure 5, although we see that there is an overlap between all the groups, the maximum of the total strain energy density is significantly different ($p < 0.01$) between the groups (see Table 4b in the Appendix). This overlap is also visible in the cumulative distribution function plot on the right, where the functions of the first and second group intersect on the top, and the third and fourth group almost intersect. From the cumulative distribution functions we can estimate the probabilities of reaching a certain amount of maximum total strain. For example, this figure suggests that with 80% probability a

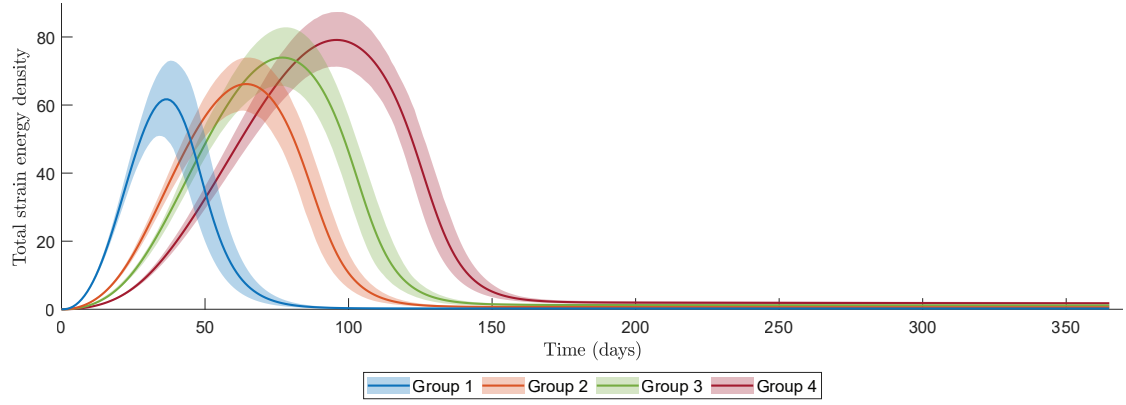


Figure 7: Confidence intervals for the strain energy in the healing of burns in different age groups. The intervals show the mean values and the 95% confidence values of the mean

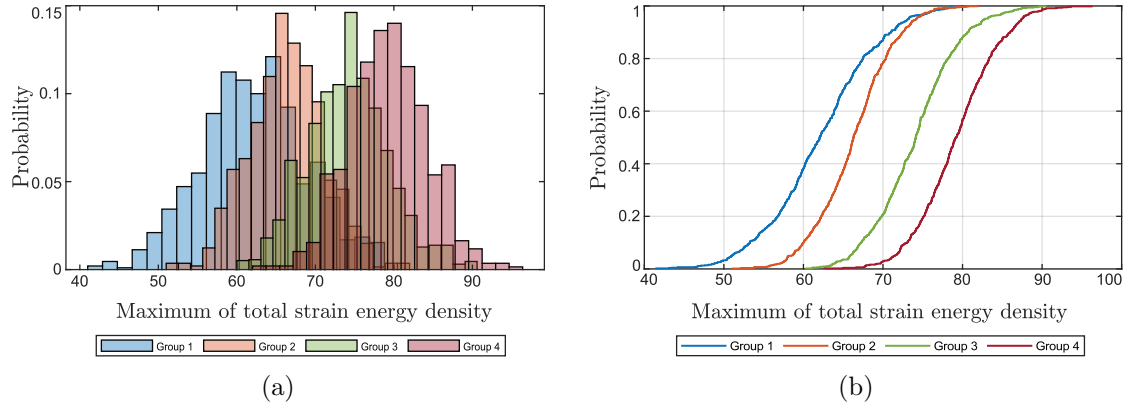


Figure 8: Histograms of the maximum of the total strain energy density (a) and its cumulative distribution function (b)

patient from groups of patients 1, 2, 3, and 4, respectively, can reach a maximum of 67.5, 70.4, 72, and 83.3 total strain.

7 Discussion

In this study, we worked with the morphoelastic model for contraction and contractures in burn scars. This model was developed by Koppenol, and based on the principle of morphoelasticity described by Hall (2008). We have provided a one-dimensional version of this model and focused on the parameter values, the sensitivity of the parameter values, and the feasibility of the model for patients of different ages.

We comprehensively described the (ranges of the) values of the parameters. Most of the variety in the parameter values we have found in literature sources. We estimated some

parameter values and adopted other parameter values from Koppenol. In case there were ranges of values found in literature, we chose upper or lower bounds, or a fixed value in between. We have used these values as mean values for the sensitivity analysis and for the parameters we have used for the second age group in our feasibility study.

For our sensitivity analysis, we varied 30 parameters by $\pm 0, 5, 10, 15, 20, 25\%$, and we varied the length of the initial wound. We showed results for the minimum of the relative surface area, the day on which wound healing reached this minimum, the relative surface area on day 365, the maximum value of the strain energy density, and the day on which wound healing reaches this maximum. The most sensitive parameter is the equilibrium collagen concentration present in the dermal layer. Other parameters that seem significantly sensitive are the apoptosis rate of fibroblasts, the apoptosis rate of myofibroblasts, the constant R in equation (15) that influences the body force, and the secretion rate of signaling molecules. The parameters we found to be the least sensitive are the fluxes parameters, the crowding factor, the viscosity, the mass density of dermal tissue, and the initial collagen concentration. We note that we let the initial collagen concentration depend on the equilibrium collagen concentration, which can influence the sensitivity value of this parameter.

Furthermore, we performed a feasibility study for the model to investigate the effect of aging on contraction, contractures and discomfort in burn wound healing. We have chosen for four groups of patients in age classes: 0-15, 16-40, 41-70, 70+. We varied the parameters of the model according to observations from the literature, so that there was a variation between the groups of patients. We furthermore varied the parameters of the model using Karhunen-Loève expansions, to model the heterogeneity of human skin, and in the framework of our Monte Carlo method we performed sampling from statistical distributions to assess the impact of uncertainty in the data on the behavior of contraction. The model is feasible for this approach, showing that contraction increases with age, that the maximum amount of contraction happens later in elderly people (showing delayed healing), that there is more contracture in elderly people, and that the variety of contracture formation is larger in elderly people than in children. Next to these results, we see that the extent of discomfort is highly related to the contraction in wound healing. The figures show that there is a larger amount of discomfort in elderly patients and that the maximum discomfort is experienced significantly ($p < 0.001$) earlier in younger children than in other age groups.

This study confirms that contraction increases with age and shows that there is a significant difference ($p < 0.001$) in maximum amount of contraction between the different age groups. The least significant difference is found between ages 0-15 and 16-40, which can also be seen in Figure 4. Further, the differences in the amount of contraction on day 365 in consecutive groups is least significant between 41-70 and 70+ years (see Table 4c in the Appendix). The most significant difference in the amount of contraction on day 365 in consecutive groups is found to be between 0-15 and 16-40 years. Given the cumulative distribution functions, we can give probabilities of a certain amount of contraction in specific age-dependent groups of patients. We have seen that the differences in the

maximum contraction and the contraction on day 365 are of a few percentages (less than 10) of order. For the maximum discomfort that a patient might feel, we have seen that there is significant difference ($p < 0.001$) between all groups, of which in consecutive groups the difference between ages 16-40 and 41-70 is most significant. From the figures we can conclude that these patients experience the same amount of discomfort, although this happens much quicker in children.

However, we note that we obtained the results with a mathematical model for which it is hard to find validation data. In the clinic, contraction is of less order in elderly patients and the retraction takes a longer period. Furthermore, contraction in children happens in a different way than in adults because of the growth. This leads to different problems in children which we did not take into account in this model. Therefore we conclude only that the model could be feasible for an age-related study for contraction in dermal wound healing and for that, the model needs further adjustments.

Further research is needed to understand the differences that appear in contraction between the various age classes of patients. We therefore plan on adding another factor to equation (16) to account for the growth of children. One other option is to put time-dependence on (some of) the parameters and simulate for a much longer time period. For example, the skin collagen content decreases at about 2% per year (Farage et al., 2015) and that has the most influence on the time healing period and amount of contraction. In order to incorporate more geometrical matters, it is necessary to extend the model to a more-dimensional framework. Though more-dimensional frameworks allow to assess geometrical issues, these more-dimensional frameworks will require more simulation time and the use of a more advanced computer infrastructure if the objective is to carry out Monte Carlo simulations for the assessment of the likelihood that contractions of a particular intensity occur. As we have mentioned earlier in our previous work, we want to incorporate hypertrophy to this one-dimensional morphoelastic model. The incorporation of hypertrophy will quickly provide new results and therefore insight, because of the high computational speed of the one-dimensional model. Furthermore, we want to model the boundaries of the wounded area as elastic springs, where we would model

$$\frac{1}{K_{spring}} \underline{\sigma} \cdot \mathbf{n} + \mathbf{u} = 0. \quad (38)$$

A further step in this research area will be the coding of the two-dimensional model which combines contraction and hypertrophy and perform a sensitivity and feasibility study on the combined model. In two- and three-dimensional problems, the computation time increases quickly. Hence it would be an improvement to code the finite element solution to the model in a high level programming language such as C++. We plan to assess these issues in future work.

Acknowledgements

The authors are grateful for the financial support by the Dutch Burns Foundation under Project 17.105.

Appendix

Parameter	μ	Parameter	μ	σ
\overline{M}	0	a_c^I	10^{-8}	3.45×10^{-10}
\bar{c}	0	a_c^{II}	10^{-8}	6.25×10^{-10}
\tilde{c}	10^{-8}	a_c^{IV}	10^{-9}	10^{-10}
δ_M	6×10^{-2}	ξ	4.4×10^{-2}	1.1×10^{-3}
R	0.995	δ_c	5×10^{-4}	9.8×10^{-6}
r_F^{\max}	2	k_c	3×10^{-13}	3.95×10^{-15}
η^I	2	ρ_t	1.09	1.21×10^{-1}
η^{II}	0.45	χ_F	2×10^{-3}	2.22×10^{-4}
k_ρ^{\max}	10			

(a) Constant along patients, constant along domain

Parameter	μ^1	μ^2	μ^3	μ^4
\overline{N}	1.5×10^4	10^4	9.5×10^3	9×10^3
$\bar{\rho}$	1.25×10^{-1}	1.125×10^{-1}	1.05×10^{-1}	9.75×10^{-2}

(b) Constant along patients, varied along domain

(c) Varied along patients, constant along domain

Param.	μ^1	μ^2	μ^3	μ^4	σ
D_F	1.2×10^{-6}	10^{-6}	8.5×10^{-7}	7×10^{-7}	1.43×10^{-7}
D_c	3.25×10^{-3}	2.88×10^{-3}	2.55×10^{-3}	2.2×10^{-3}	3.2×10^{-4}
r_F	1.222	9.24×10^{-1}	8.16×10^{-1}	6.11×10^{-1}	7.11×10^{-2}
κ_F	10^{-6}	10^{-6}	1.5×10^{-6}	2×10^{-6}	1.11×10^{-7}
k_F	1.14×10^7	1.08×10^7	1.02×10^7	9.63×10^6	5.68×10^5
a_c^{III}	2.05×10^8	2×10^8	1.95×10^8	1.9×10^8	4.35×10^6
δ_N	1.9×10^{-2}	2×10^{-2}	2.1×10^{-2}	2.2×10^{-2}	2.27×10^{-4}
δ_ρ	6.11×10^{-6}	6×10^{-6}	5.89×10^{-6}	5.78×10^{-6}	1.09×10^{-7}
μ	10^2	10^2	1.2×10^2	1.4×10^2	1.11×10
E	3.2×10^2	3.5×10^2	3.8×10^2	4.1×10^2	1.03×10
ζ	3.8×10^2	4×10^2	4.2×10^2	4.4×10^2	1.82×10

(d) Varied along patients, varied along domain

Table 3: Parameter values. In subtables (c) and (d), $\mu^i, i \in \{1, 2, 3, 4\}$ denotes the mean value in class i of patients of different age

Groups	t -value	Groups	t -value	Groups	t -value
1&2	17	1&2	23	1&2	167
1&3	58	1&3	63	1&3	273
1&4	94	1&4	91	1&4	385
2&3	43	2&3	49	2&3	126
2&4	80	2&4	83	2&4	241
3&4	36	3&4	32	3&4	108

(a) The values of the t -statistic comparing the minima of the relative surface area between age groups

(b) The values of the t -statistic comparing the maxima of total strain between age groups

(c) The values of the t -statistic comparing the relative surface area on day 365 between age groups

Table 4: The values of the t -statistic comparing the minima of the relative surface area (a), the maxima of the total strain (b) and the relative surface area on day 365 (c)

References

- Alberts, B., Bray, D., Lewis, J., Raff, M., Roberts, K., and Watson, J. (1989). *The Molecular Biology of The Cell*. Garland Publishing, second edition.
- Ashcroft, G. S., Horan, M. A., Herrick, S. E., Tarnuzzer, R. W., Schultz, G. S., and Ferguson, M. W. J. (1997). Age-related differences in the temporal and spatial regulation of matrix metalloproteinases (MMPs) in normal skin and acute cutaneous wounds of healthy humans. *Cell and Tissue Research*, 290(3):581–591.
- Azzarone, B., Faily Crepin, C., Daya Grosjean, L., Chaponnier, C., and Gabbiani, G. (1983). Abnormal behavior of cultured fibroblasts from nodule and nonaffected aponeurosis of dupuytren’s disease. *Journal of Cellular Physiology*, 117(3):353–361.
- Barocas, V. H. and Tranquillo, R. (1997). An Anisotropic Biphasic Theory of Tissue-Equivalent Mechanics: The Interplay Among Cell Traction, Fibrillar Network Deformation, Fibril Alignment, and Cell Contact Guidance. *Journal of Biomechanical Engineering*, 119(2):137–145.
- Bowen-Pope, D., Malpass, T., Foster, D., and Ross, R. (1984). Platelet-derived growth factor in vivo: levels, activity, and rate of clearance. *Blood*, 64(2):458–469. PMID: 6331547 indexed for MEDLINE.
- Dallon, J., Sherrat, J., and Maini, P. (1999). Mathematical Modelling of Extracellular Matrix Dynamics Using Discrete Cells: Fiber Orientation and Tissue Regeneration. *Journal of Theoretical Biology*, 199(4):449–471.
- Desmoulière, A., Geinoz, A., Gabbiani, F., and Gabbiani, G. (1993). Transforming growth factor-beta 1 induces alpha-smooth muscle actin expression in granulation tissue myofibroblasts and in quiescent and growing cultured fibroblasts. *The Journal of Cell Biology*, 122(1):103–111.

- Dziuk, G. and Elliot, C. (2007). Finite elements on evolving surfaces. *IMA Journal of Numerical Analysis*, 27(2):262–292.
- Egberts, G., Vermolen, F., and van Zuijlen, P. (2020). A one-dimensional morphoelastic model for burn injuries: stability, numerical validation, and biological interpretation.
- Enoch, S. and Leaper, D. (2008). Basic Science of Wound Healing. *Surgery (Oxford)*, 26(2):31–37.
- Farage, M. A., Miller, K. W., and Maibach, H. I. (2015). Degenerative Changes in Aging Skin. In *Textbook of Aging Skin*, pages 1–18. Springer Berlin Heidelberg.
- Garrison, G., Huang, S. K., Okunishi, K., Scott, J. P., Penke, L. R. K., Scruggs, A. M., and Peters-Golden, M. (2013). Reversal of myofibroblast differentiation by prostaglandin e2. *American Journal of Respiratory Cell and Molecular Biology*, 48(5):550–558.
- Goel, A. and Shrivastava, P. (2010). Post-burn scars and scar contractures. *Indian Journal of Plastic Surgery*, 43(3):63.
- Gosh, K., Pan, Z., Guan, E., Ge, S., Lio, Y., Nakamura, T., Ren, Z. D., Rafailovich, M., and Clark, R. (2007). Cell Adaptation to a Physiologically Relevant ECM Mimic with Different Viscoelastic Properties. *Biomaterials*, 28(4):671–679.
- Grotendorst, G. (1992). *Chemoattractants and growth factors*, chapter 15, pages 237–246. W.B. Saunders, Philadelphia, Pennsylvania, 1 edition. In: Cohen 1, Diegelmann R, Lindblad W (eds) Wound Healing: Biochemical and Clinical Aspects.
- Gunin, G., Kornilova, N., Petrov, V., and Vasilyeva, O. (2011). Age changes in the number and proliferation of fibroblasts in the human skin. *Advances in Gerontology*, 1(4):299–303.
- Hall, C. L. (2008). *Modelling of some biological materials using continuum mechanics*. PhD thesis, Queensland University of Technology.
- Harper, R. and Grove, G. (1979). Human skin fibroblasts derived from papillary and reticular dermis: differences in growth potential in vitro. *Science*, 204(4392):526–527.
- Haugh, J. M. (2006). Deterministic model of dermal wound invasion incorporating receptor-mediated signal transduction and spatial gradient sensing. *Biophysical Journal*, 90(7):2297–2308.
- Javierre, E., Moreo, P., Doblaré, M., and García-Aznar, J. (2009). Numerical modeling of a mechano-chemical theory for wound contraction analysis. *International Journal of Solids and Structures*, 46(20):3597–3606.
- Koppenol, D. C. (2017). *Biomedical implications from mathematical models for the simulation of dermal wound healing*. PhD thesis, Delft University of Technology.

- Koppenol, D. C. and Vermolen, F. J. (2017). Biomedical implications from a morphoelastic continuum model for the simulation of contracture formation in skin grafts that cover excised burns. *Biomechanics and Modeling in Mechanobiology*, 16(4):1187–1206.
- Koppenol, D. C., Vermolen, F. J., Niessen, F. B., van Zuijlen, P. P. M., and Vuk, K. (2016). A mathematical model for the simulation of the formation and the subsequent regression of hypertrophic scar tissue after dermal wounding. *Biomechanics and Modeling in Mechanobiology*, 16(1):15–32.
- Krueger, N. and Luebberding, S. (2017). *Age-Related Changes in Skin Mechanical Properties in Textbook of Aging Skin*, pages 309–317. Springer-Verlag Berlin Heidelberg.
- Lang, T. C., Zhao, R., Kim, A., Wijewardena, A., Vandervord, J., Xue, M., and Jackson, C. J. (2019). A Critical Update of the Assessment and Acute Management of Patients with Severe Burns. *Advances in Wound Care*, 8(12):607–633.
- Maskarinec, S., Franck, C., Tirell, D., and Ravichandran, G. (2009). Quantifying cellular traction forces in three dimensions. *Proceedings of the National Academy of Sciences*, 106(52):22108–22113.
- McDougall, S., Dallon, J., Sherratt, J., and Maini, P. (2006). Fibroblast Migration and Collagen Deposition during Dermal Wound Healing: Mathematical Modelling and Clinical Implications. *Philosophical Transactions of the Royal Society A: Mathematical, Physical and Engineering Sciences*, 364(1843):1385–1405.
- Miller, C. C., Godeau, G., Lebreton-DeCoster, C., Desmouliere, A., Pellat, B., Dubertret, L., and Coulomb, B. (2003). Validation of a morphometric method for evaluating fibroblast numbers in normal and pathologic tissues. *Experimental Dermatology*, 12(4):403–411.
- Moulin, V., Larochelle, S., Langlois, C., Thibault, I., Lopez-Vallé, C. A., and Roy, M. (2003). Normal skin wound and hypertrophic scar myofibroblasts have differential responses to apoptotic inductors. *Journal of Cellular Physiology*, 198(3):350–358.
- Moulin, V., Mayrand, D., Laforce-Lavoie, A., Larochelle, S., and Genest, H. (2011). *Regenerative Medicine and Tissue Engineering - Cells and Biomaterials*, chapter Chapter 8, pages 195–208. IntechOpen.
- Murphy, K., Hall, C., Maini, P., McCue, S., and MacElwain, D. (2012). A fibrocontractive mechanochemical model of dermal wound closure incorporating realistic growth factor kinetics. *Bulletin of Mathematical Biology*, 74(5):1143–1170.
- Murray, J. D. (2011). *Mathematical Biology II*. Springer New York.
- Olsen, L., Sherratt, J., and Maini, P. (1995). A Mechanochemical Model for Adult Dermal Wound Contraction and the Permanence of the Contracted Tissue Displacement Profile. *Journal of Theoretical Biology*, 177(2):113–128.
- Overall, C., Wrana, J., and Sodek, J. (1991). Transcriptional and post-transcriptional

- regulation of 72-kda gelatinase/ type iv collagenase by transforming growth factor-beta in human fibroblasts. *Journal of Biological Chemistry*, 266(21):14061–14071.
- Pawlaczyk, M., Lelonkiewicz, M., and Wieczorowski, M. (2013). Age-dependent biomechanical properties of the skin. *Advances in Dermatology and Allergology*, 5:302–306.
- Pond, D., McBride, A., Davids, L., Reddy, B., and Limbert, G. (2018). Microstructurally-based constitutive modelling of the skin – linking intrinsic ageing to microstructural parameters. *Journal of Theoretical Biology*, 444:108–123.
- Ramtani, S. (2004). Mechanical modelling of cell/ecm and cell/cell interactions during the contraction of a fibroblast-populated collagen microsphere: theory and model simulation. *Journal of Biomechanics*, 37(11):1709–1718.
- Ramtani, S. and et al (2002). Remodeled-matrix contraction by fibroblasts: numerical investigations. *Computers in Biology and Medicine*, 32(4):283–296.
- Randolph, R. K. and Simon, M. (1998). Dermal fibroblasts actively metabolize retinoic acid but not retinol. *Journal of Investigative Dermatology*, 111(3):478–484.
- Roberts, A., Sporn, M., Assoian, R., Smith, J., Roche, N., Wakefield, L., Heine, U., Liotta, L., Falanga, V., Kehrl, J., and Fauci, A. (1986). Transforming growth factor type beta: Rapid Induction of Fibrosis and Angiogenesis in Vivo and Stimulation of Collagen Formation in Vitro. *Proceedings of the National Academy of Sciences*, 83(12):4167–4171.
- Rudolph, R. and Vande Berg, J. (1991). The myofibroblast in Dupuytren’s contracture. *J. Hand Clinics*, 7(4):683–692. Discussion 693–4.
- Sillman, A., Quang, D., Farboud, B., Fang, K., Nuccitelli, R., and Isseroff, R. (2003). Human dermal fibroblasts do not exhibit directional migration on collagen i in direct-current electric fields of physiological strength. *Experimental Dermatology*, 12(4):396–402.
- Simpson, M., Lo, K., and Sun, Y. (2017). Quantifying the roles of random motility and directed motility using advection-diffusion theory for a 3t3 fibroblast cell migration assay stimulated with an electric field. *BMC Systems*, 11(1):39.
- Simpson, R., Meran, S., Thomas, D., Stephens, P., Bowen, T., Steadman, R., and Phillips, A. (2009). Age-related changes in pericellular hyaluronan organization leads to impaired dermal fibroblast to myofibroblast differentiation. *The American Journal of Pathology*, 175(5):1915–1928.
- Strutz, F. e. a. (2001). Tgf- β 1 induces proliferation in human renal fibroblasts via induction of basic fibroblast growth factor (fgf-2). *Kidney International*, 59(2):579–592.
- Tiwari, V. K. (2012). Burn wound: How it differs from other wounds? *Indian Journal of Plastic Surgery*, 45(02):364–373.

- Tranquillo, R. and Murray, J. D. (1992). Continuum Model of Fibroblast-Driven Wound Contraction: Inflammation-Mediation. *Journal of Theoretical Biology*, 158(2):135–172.
- Van Kan, J., Segal, A., and Vermolen, F. (2014). *Numerical Methods in Scientific Computing*. Delft Academic Press, 2nd edition.
- Vande Berg, J., Rudolph, R., Poolman, W., and Disharoon, D. (1989). Comparative growth dynamics and actin concentration between cultured human myofibroblasts from granulating wounds and dermal fibroblasts from normal skin. *Lab Invest*, 61(5):532–538.
- Wakefield, L. M., Winokur, T. S., Hollands, R. S., Christopherson, K., Levinson, A. D., and Sporn, M. B. (1990). Recombinant latent transforming growth factor beta 1 has a longer plasma half-life in rats than active transforming growth factor beta 1, and a different tissue distribution. *Journal of Clinical Investigation*, 86(6):1976–1984.
- Wiegand, C., Raschke, C., and Elsner, P. (2017). *Textbook of Aging Skin*, chapter 6, pages 55–65. Springer, Berlin, Heidelberg. Skin Aging: A Brief Summary of Characteristic Changes.
- Wrobel, L., Fray, T., Molloy, J., Adams, J., Armitage, M., and Sparrow, J. (2002). Contractility of Single Human Dermal Myofibroblasts and Fibroblasts. *Cell Motility and the Cytoskeleton*, 52(2):82–90.
- Wrobel, L., Fray, T., Molloy, J., Adams, J., Armitage, M., and Sparrow, J. (2009). Anex A: Table A.1. *Annals of the ICRP Publication 110*, 39(2):48–51.
- Xu, F. and Tianjian, L. (2011). *Introduction to Skin Biothermomechanics and Thermal Pain*. Springer.
- Yang, L., Qiu, C. X., Ludow, A., Ferguson, M. W., and Brunner, G. (1999). Active transforming growth factor-beta in wound repair. *The American Journal of Pathology*, 154(1):105–111.
- Young, A. and McNaught, C. (2011). The Physiology of Wound Healing. *Surgery (Oxford)*, 29(10):475–479.